Three-dimensional bottom diffraction in the North Pacific

Ralph A. Stephen, S. Thompson Bolmer, Peter F. Worcester, Matthew A. Dzieciuch, and Ilya A. Udovydchenkov

Citation: The Journal of the Acoustical Society of America **146**, 1913 (2019); doi: 10.1121/1.5125427
View online: https://doi.org/10.1121/1.5125427
View Table of Contents: https://asa.scitation.org/toc/jas/146/3
Published by the Acoustical Society of America

Three-dimensional bottom diffraction in the North Pacific

Ralph A. Stephen[a] and S. Thompson Bolmer
Woods Hole Oceanographic Institution, Woods Hole, Massachusetts 02543, USA

Peter F. Worcester and Matthew A. Dzieciuch
Scripps Institution of Oceanography, La Jolla, California 92093-0225, USA

Ilya A. Udovydchenkov
MITRE Corporation, Bedford, Massachusetts 01730, USA

(Received 29 June 2018; revised 16 November 2018; accepted 3 January 2019; published online 1 October 2019)

A significant aspect of bottom-interaction in deep water acoustic propagation, from point sources to point receivers, is the diffraction (or scattering) of energy from discrete seafloor locations along repeatable, deterministic paths in three-dimensions. These bottom-diffracted surface-reflected (BDSR) paths were first identified on the North Pacific acoustic laboratory experiment in 2004 (NPAL04) for a diffractor located on the side of a small seamount. On the adjacent deep seafloor, ambient noise and propagation in the ocean sound channel were sufficiently quiet that the BDSRs were the dominant arrival. The ocean bottom seismometer augmentation in the North Pacific (OBSANP) experiment in June–July 2013 studied BDSRs at the NPAL04 site in more detail. BDSRs are most readily identified by the arrival time of pulses as a function of range to the receiver for a line of transmissions. The diffraction points for BDSRs occur on the relatively featureless deep seafloor as well as on the sides of small seamounts. Although the NPAL04 and OBSANP experiments had very different geometries the same diffractor location is consistent with observed arrivals in both experiments within the resolution of the analysis. On OBSANP the same location excites BDSRs for 77.5, 155, and 310 Hz transmissions.
https://doi.org/10.1121/1.5125427

[YTL] Pages: 1913–1922

I. INTRODUCTION

Interaction with the seafloor is a significant aspect of short- and long-range ocean acoustic propagation (source to receiver separations from zero to thousands of kilometers). For impulsive sources, in addition to specular reflections and random scattering from the seafloor, a significant aspect of bottom-interacting acoustics in deep water is diffraction (or deterministic scattering) of energy from discrete seafloor locations along repeatable paths in three-dimensions (Stephen *et al.*, 2009; Stephen *et al.*, 2013). These bottom-diffracted surface-reflected (BDSR) paths are distinct from bottom-reflected surface-reflected (BRSR) paths (Munk *et al.*, 1995) because the emergence angle from the seafloor is not equal to the angle of incidence given the resolvable bathymetry (about 200 m resolution). BDSRs are important for at least four reasons: (i) they provide a mechanism for signals and noise from distant sources to penetrate into shadow zones (created for example by simple focusing in the sound channel or by bathymetric blockage), (ii) for long-range transmissions to the deep seafloor they can be the largest amplitude arrival, (iii) their presence suggests that deep seafloor ambient noise and signal-to-noise ratios can be a function of local topography around the receivers, and (iv) they are the reciprocal of the T-phase excitation problem in marine seismology (Butler and Lomnitz, 2002; Chapman and Marrett, 2006; de Groot-Hedlin and Orcutt, 1999; Okal, 2008; Williams *et al.*, 2006; Yang and Forsyth, 2003).

BDSRs are not modeled by current propagation codes and the geological features responsible for BDSRs are poorly understood. Diffractors can be located on the relatively featureless abyssal seafloor as well as on the sides of small seamounts and they are commonly located out of the sagittal plane. ("Sagittal" comes from the Latin word for arrow and the sagittal plane is the plane between source and receiver in which an arrow would ideally fly, i.e., the vertical plane between source and receiver.)

Using data from the North Pacific acoustic laboratory experiment in 2004 (NPAL04), Stephen *et al.* (2009) and Stephen *et al.* (2013) showed for deep water, long-range propagation that BDSR arrivals are observed throughout the water column but that at receivers near the seafloor they can be significantly larger, in some cases by as much as 20 dB, than the arrivals that travelled through the ocean sound channel directly to the seafloor. At 3200 km range, the direct ocean sound channel arrivals were not observed at all on the seafloor and the only observed arrivals followed BDSR paths. Triangulation of the BDSR arrival times at three of the ocean bottom seismometers at about 5000 m depth located the principal diffractor on the side of Seamount B, at a depth of about 4250 m, about 18 km from the receivers and offset laterally more than 2 km from the source–receiver geodesic.

In this paper we present observations from the ocean bottom seismometer augmentation in the North Pacific (OBSANP) experiment that was carried out in June and July

[a]Also at: RASCON Associates, Falmouth, Massachusetts 02540, USA. Electronic mail: rstephen@whoi.edu

2013 (Stephen *et al.*, 2014) at the same receiver site as NPAL04. Using transmissions from a pattern of radial lines out to 50 km we show that BDSRs can be readily identified by their arrival time as a function of source–receiver range. In an area within about 25 km of the receivers 45 diffractor locations were identified. Some are on the side of small seamounts, but most occurred in the relatively featureless, flat seafloor and some are in the sagittal plane (i.e., in two dimensions) but most are located out of the sagittal plane (i.e., in three-dimensions). The NPAL04 diffractor location, that excited BDSRs at ranges of 500–3200 km, can also explain one of the OBSANP BDSRs (called "p"), excited at ranges less than 50 km, within the resolution of the experiments. To quantify the geometry for future modeling efforts, the ranges and azimuths for excitation and scattering of the observed BDSR from "p" are presented. The same BDSR from "p" can be observed for 77.5, 155, and 310 Hz transmissions.

Some topics related to the NPAL04 and OBSANP experiments are discussed in Sec. VII. These include: (i) the various resolutions involved in the experiments, (ii) some ideas on the actual diffraction mechanism responsible for BDSRs, (iii) a comparison of long- and short-range BDSRs, (iv) some suggestions for future work, and (v) an explanation of the T-phase problem in marine seismology. A note on the semantics of "diffraction" and "scattering" as used in this paper is given in the Appendix.

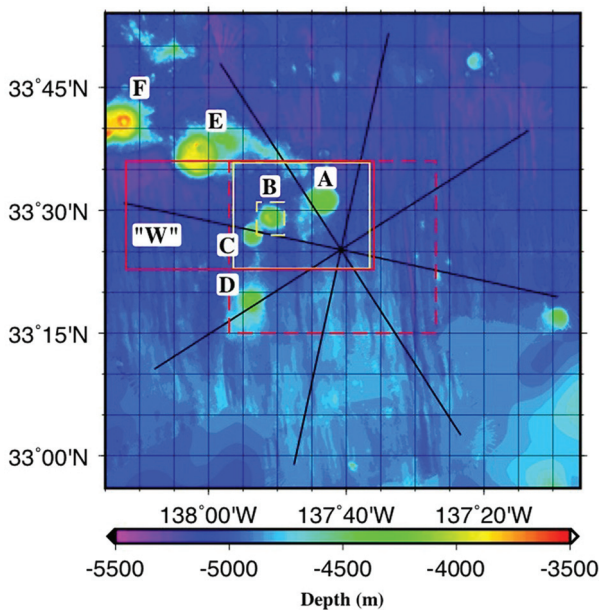

FIG. 1. The location of the eight, 50 km long, radial underway transmission lines (solid, black lines) superimposed on the regional bathymetry. The radial lines intersect at the location of the deep vertical line array (DVLA). The merged multi-beam data has been gridded to a 200 m resolution. The four rectangular boxes show the location of later figures in the paper: Fig. 2—solid yellow box, Fig. 4—dashed red box, Fig. 6—solid red box, and Fig. 8—dashed yellow box.

II. THE OBSANP EXPERIMENT

One goal of the OBSANP experiment in June and July 2013 (Stephen *et al.*, 2014) was to identify and study the characteristics of BDSR arrivals occurring at short ranges (less than 50 km) including their frequency dependence in the band from 50 to 400 Hz. Since BDSR arrivals had been observed in the NPAL04 experiment at ranges from 500 to 3200 km, the OBSANP experiment tested the hypothesis that BDSR paths contribute significantly to the arrival structure on the deep seafloor even at short ranges. On OBSANP we deployed a 32 element deep vertical line array (DVLA) from 12 to 987 m above the seafloor, eight short-period ocean bottom seismometers (OBSs) and four long-period OBSs and we carried out a 15 days transmission program using a J15-3 acoustic source towed from a ship. The experiment consisted of four phases: (i) an ambient noise phase spanning the band from 0.03 to 700 Hz (Farrell *et al.*, 2016; Berger *et al.*, 2018), (ii) an array of station stops within 50 km of the receivers, (iii) a long line of station stops and underway transmissions to 250 km from the receivers along the same geodesic as the NPAL04 experiment, and (iv) eight radial underway transmission lines out to 50 km range at an azimuthal separation of 45 deg. Since BDSRs are most easily identified, and the diffractors are most easily located, using the arrival time versus range information for lines of transmissions, this paper addresses the analysis of data from the eight radial underway lines (Fig. 1).

The constellation of receivers consisted of: (i) a 32-hydrophone DVLA, at hydrophone module heights ranging from 12 to 987 m above the seafloor, (ii) four short-period OBSs deployed about 2 km from the DVLA (SP1, SP2, SP3, and SP4), (iii) four broadband seismometers deployed about 4 km from the DVLA (LPA, LPB, LPC, and LPD), and (iv) four short-period seismometers deployed towards the seamounts to the west of the DVLA (SP5, SP6, SP7, and SP8) (Fig. 2). All instruments were successfully recovered at the end of the cruise.

Each of the short-period seismometers had three inertial channels (vertical and two horizontal Mark Products L22 28-Hz geophones) and a hydrophone channel (HTI-90-U). These are typically used in controlled-source seismic refraction experiments with a target bandwidth from 10 to 200 Hz. Six of the short-period seismometers (SP1, SP2, SP3, SP4,

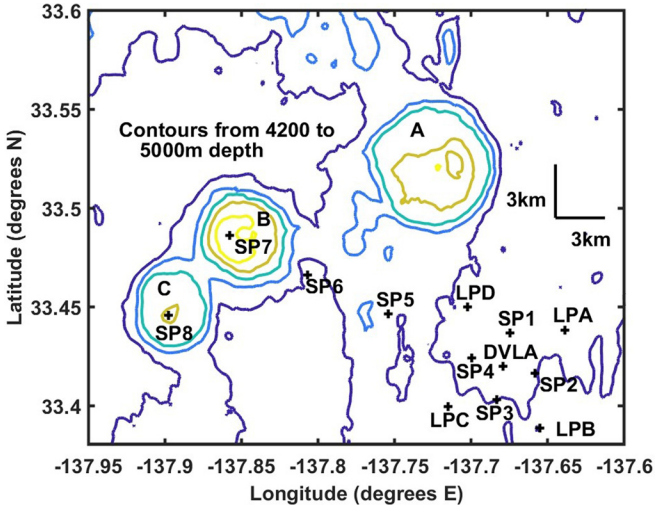

FIG. 2. (Color online) Locations of the eight short period OBSs (SP*), the four long period OBSs (LP*), and the OBSANP DVLA with respect to the bathymetric relief.

SP7, and SP8) had additional self-recording hydrophone modules identical to the hydrophone modules in the DVLA.

The four long-period seismometers had three inertial channels (Trillium 240 seismometers) and a differential pressure gauge. These are typically used for earthquake and ambient noise studies with a target bandwidth from 0.005 to 10 Hz. Two long-period seismometers (LPB and LPD) had an additional broadband ultra-low-noise hydrophone channel (ULN-SAIC) (Berger *et al.*, 2018).

The hydrophone modules sampled at 1953.125 sps (samples per second) and all of the OBS channels were sampled at 1000 sps. The locations and water depths of all the receivers are given in Table I.

Some of the deployed sensors did not return useful data. Five of the hydrophone modules on the DVLA, between 937 and 977 m above the seafloor, did not record data. OBS SP1 had bad timing on the three inertial and hydrophone channels. OBS SP7 did not record data for the three inertial and hydrophone channels. Fortunately both SP1 and SP7 had autonomously recording hydrophone modules on board and these returned useful data for these sites. The differential pressure gauge on LPD did not acquire useful data but this OBS did have an SAIC hydrophone to provide broadband acoustic data. So of the 83 expected channels, 69 channels were available for analysis.

Along the eight radial lines centered at the DVLA, acoustic signals were transmitted at nominal frequencies of 77.5, 155, and 310 Hz. The "west line" ("W") coincides with the geodesic from the sources to the DVLA on NPAL04 (Mercer *et al.*, 2009; Stephen *et al.*, 2014).

The radial line experiment acquired a large data set. There are 1656 arrival time plots, like Fig. 3 below, to review for BDSRs (69 channels, three frequencies, eight lines). For each of the eight radial lines there were about 167 transmissions at each of the three frequencies. These generated 276 552 traces (which required 1 106 208 replica correlations). All transmissions also required accurate navigation and timing information.

Voltages and currents from the power amplifier to the J15-3 acoustic source (parameters used to predict sound pressure level), acoustic pressure levels at a monitor hydrophone suspended near the J15-3, and the depth of the source were monitored continuously throughout the experiment (McPeak *et al.*, 2013). Care was taken to excite the J15-3 as loudly as possible without distortion. A typical undistorted source level for the J15-3 in the band from 75 to 250 Hz is 172 dB re 1 μPa at 1 m. While underway at 2 knots, the source was towed at a nominal depth of 60 m. At station stops (not discussed in this paper) the source was suspended at a depth of 100 m.

TABLE I. OBSANP instrument locations and depths.

Instrument	Latitude °N	Longitude °E	Depth (m)
DVLA	33.4200	−137.6793	5048
LPA	33.4384	−137.6387	5049
LPB	33.3887	−137.6550	4996
LPC	33.3995	−137.7153	4933
LPD	33.4497	−137.7025	5047
SP1	33.4368	−137.6746	5076
SP2	33.4163	−137.6584	5023
SP3	33.4029	−137.6832	5004
SP4	33.4240	−137.6998	5018
SP5	33.4462	−137.7539	4956
SP6	33.4661	−137.8069	5018
SP7	33.4861	−137.8576	4024
SP8	33.4455	−137.8975	4392

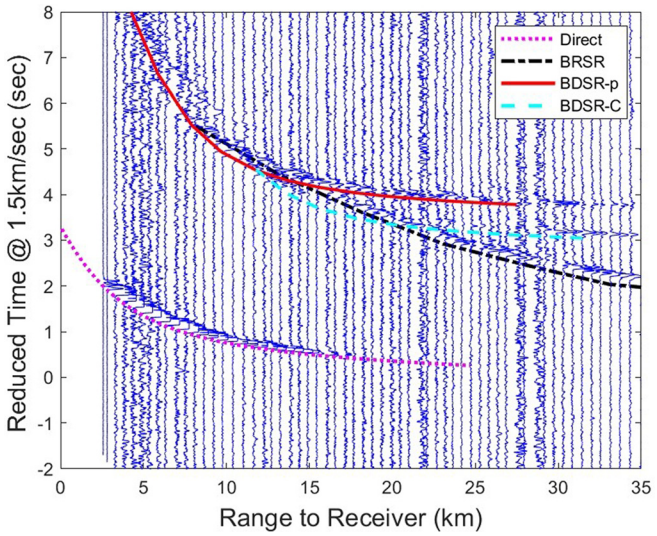

FIG. 3. (Color online) Computed arrival times for direct, BRSR, BDSR-p, and BDSR-C are overlain on the received traces for 77.5 Hz transmissions on the West line to the Ocean Bottom Seismometer SP6 (vertical component, shaded circle in Fig. 4). The BDSR from the NPAL04 diffraction point (BDSR-p, solid line, shaded square in Fig. 4) is observed at ranges from 15 to 35 km. There is also a BDSR scattered from a location on Seamount C (BDSR-C, dashed line, shaded diamond in Fig. 4). The amplitude of the BDSR arrivals is of the same order as the amplitude of the BRSR arrival.

A useful summary of the transmission strategy used in long-range ocean acoustic and tomography experiments is given by Munk *et al.* (1995). A relatively low-strength, long-duration, but well-controlled, known signal, is transmitted into the water. Relatively high-amplitude, short-duration pulses are then obtained from the received signal by replica correlation (also called pulse compression or matched filtering) with the transmitted signal (Baggeroer and Kuperman, 1983; Birdsall, 1976; Birdsall and Metzger, 1986; Birdsall *et al.*, 1994; Golomb, 1982; Metzger, 1983). For the radial lines on OBSANP four periods of M-sequences (short for "binary maximal-length sequences") were transmitted at frequencies of 77.5, 155, and 310 Hz continuously on a 5 min duty cycle. Underway at 2 knots this gives spatial sampling at 0.3 km. The transmission parameters are given in Table II. For all received channels the signal-to-noise was improved by a factor of 6 dB by incoherently stacking the magnitude of the four replica-correlated traces. The magnitudes of the traces were simply summed without regard to the phase of the complex output of the correlation process. The four sequences at each frequency were not summed together prior to the replica correlation.

Although the movement of the DVLA due to currents was monitored during the experiment we assumed for this BDSR analysis that the DVLA remained vertical.

TABLE II. Transmission parameters for the radial lines.

Carrier frequency (Hz)	77.5	155	310
Transmission interval (min)	2	2	1
Number of periods	4	4	4
Duration of a period (s)	26.4	26.4	13.2
Digits per period	1023	1023	1023
Cycles per digit	2	4	4
Samples per cycle	4	4	4
Sampling frequency (sps[a])	310	620	1240
Resolution in time (ms)	26	26	13
Resolution in range (m)	40	40	20
Distance travelled at 2 knots in four periods (m)	109	109	54

[a]Samples per second.

III. BOTTOM-DIFFRACTED SURFACE-REFLECTED (BDSR) ARRIVALS

BDSRs from shallow, short-range (<50 km) pulse-like sources are readily observed on seafloor receivers in an arrival time versus range plot where their appearance varies distinctly from the appearance of BRSR paths. An example for transmissions from the west line to SP6 is shown in Fig. 3. At ranges up to 15 km or so there are just two principal arrivals: the direct wave and the BRSR (or first water multiple) wave. For this OBS at 5018 m depth the direct wave (dotted line) is not observed beyond 17 km range. Because of the focusing of sound in the ocean sound channel direct wave energy "lifts off" from the seafloor. At short ranges to SP6, the predicted arrival times for BDSR-p and BDSR-C are indistinguishable from the BRSR arrival time.

Beyond 15 km range there are three main arrivals: the BRSR and the two BDSR arrivals: BDSR-C (distinct beyond 25 km) and BDSR-p (distinct beyond 15 km). The two BDSR arrivals have comparable amplitude to the principal BRSR arrival. BDSR-p diffracted from the side of Seamount B near the same location that caused the deep seafloor arrivals from 500 to 3200 km range in the 2004 LOAPEX experiment (shaded square in Fig. 4). The diffractor for BDSR-C is directly below the west line on Seamount C (the shaded diamond in Fig. 4).

Based on the NPAL04 results, we expected to see a few BDSRs from the sides of the seamounts in the OBSANP data. Analysis of the data from the radial lines to the DVLA and all 12 ocean bottom seismometers (69 channels of data), however, revealed 45 diffractors (Fig. 4), many in the relatively flat, abyssal hill terrain away from the seamounts.

The predicted travel-time curves for BDSRs (for example in Fig. 3) are computed using ray tracing from the source at 60 m depth to a "test" BDSR location (latitude, longitude, and depth) [Fig. 5(b)] and then from the "test" location, reflecting off the sea surface, to the receiver location (latitude, longitude, and depth) [Fig. 5(c)]. All ray calculations in this paper used the same sound speed profile from a representative conductivity temperature depth (CTD) profile acquired on the cruise [Fig. 5(a)]. The CTD and expendable bathythermograph (XBT) profiles acquired are discussed in detail in Appendix G of the cruise report (Stephen *et al.*, 2014).

The primary goal of this study was simply to identify BDSR arrivals and to obtain locations. Preliminary "test"

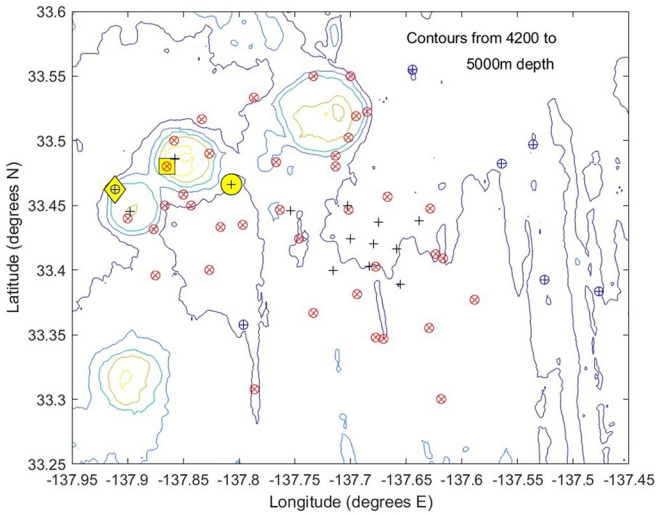

FIG. 4. (Color online) Forty-five diffractor points, identified in the OBSANP 77.5 Hz radial line data, are overlain on the multibeam bathymetry. Each BDSR appeared in a similar fashion as the example in Fig. 3 with predicted BDSR arrival time curves overlain based on the method described in the text and Fig. 5. BDSR diffraction points cannot be identified from the multibeam bathymetry. Thirty-eight are out-of-plane BDSRs (x-inscribed circles), a true three-dimensional deterministic scattering effect. Some of these diffraction points tend to cluster on the sides of seamounts but many occur on the relatively featureless deep seafloor. The seven in-plane BDSRs (+-inscribed circles) mostly occur on the featureless seafloor east of the seamounts. Diffractor "p" (shaded square), whose BDSR is indicated by the solid line in Fig. 3, is located on the side of seamount B. The receiver locations (+ symbols) are also shown. SP6, the receiver for the arrival time plot in Fig. 3, is indicated with the shaded circle. The contour interval is 200 m.

BDSR locations were guessed either by trial and error or by a coarse grid search, similar to the case in Sec. V, until suitable fits to the BDSR arrivals were obtained by eye (see the example in Fig. 3). The criterium was to fit the BDSR arrivals as well as the direct and BRSR arrivals were predicted. Quite often, BDSR arrivals were observed at incident ranges to the diffractor beyond the maximum range predicted by the ray algorithm, so a fit to these arrivals was not possible. For diffractor "p," discussed further in this paper, a fine grid of test points was chosen and the root means square (RMS) error between the computed and observed BDSR arrival times was contoured (see Sec. V below). Similar processing for all 45 diffractors in Fig. 4 would be lot of work and it is not clear at this stage that it would provide any more useful information. It may be worthwhile, in future to do similar quantitative processing on a few, select BDSRs of particular interest.

IV. BDSR-P GEOMETRY

Diffractor "p," observed for transmissions on the West line, could potentially be seen on 207 arrival time plots (like Fig. 3 for 69 receiver channels and three frequencies) but it was not observed on all of them. The source–diffractor–receiver geometry may not have been suitable; there may have been interference with the BRSR arrival or other BDSRs; there could have been poor SNR; or there were clean arrival time plots with distinct arrival times and the diffractions were simply not observed. It would be unwieldy here to show all of the arrival time plots used in the analysis of

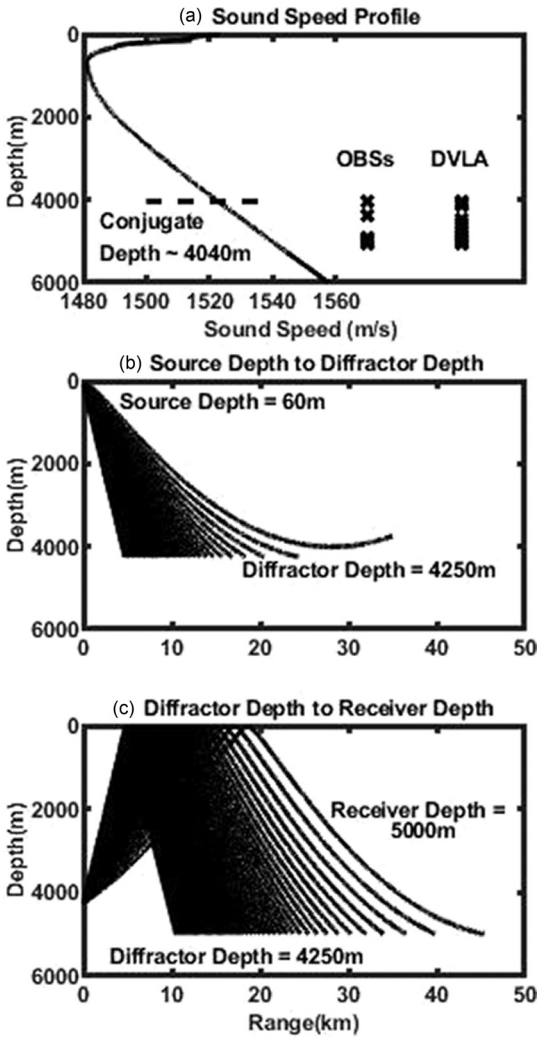

FIG. 5. (a) Sound speed profile used for the ray path calculations and BDSR diffractor locations in this paper. Depths of the DVLA hydrophones and OBSs are shown to span from the seafloor to the conjugate depth. (b) Ray paths from the source at 60 m depth to the diffractor, in this case at a depth of 4250 m. (c) Ray paths from the diffractor, here at 4250 m depth, to the receivers, in this case at 5000 m depth.

BDSR "p." The salient arrival time plots, however, are given in the supplemental material.[1]

In describing the BDSR geometry there are three relevant ranges. The first is the range between the source and the receiver at which the BDSR is observed (Fig. 3, the observed range), the second is the range between the source and the diffractor (Fig. 6, the incident range), and the third is the range between the diffractor and the receivers (Fig. 6, the diffracted or scattered range).

Diffractor "p" is ensonified by 77.5 Hz sources on the west line at observed ranges from about 25 to 45 km from OBSs SP3 (not shown, but given in the supplemental material[1]) and SP4 (Fig. 7) and from 15 to 35 km from OBS SP6 (Fig. 3). The shortest and the longest range correspond to incident ranges from 9.7 to 28.7 km from the source to diffractor "p" (Fig. 6). At long incident ranges, beyond about 25 km from the diffractor (Fig. 6), the incident energy is beyond lift-off at the diffractor [for example, Fig. 5(b)]. At these ranges it appears that the diffractor is ensonified evanescently.

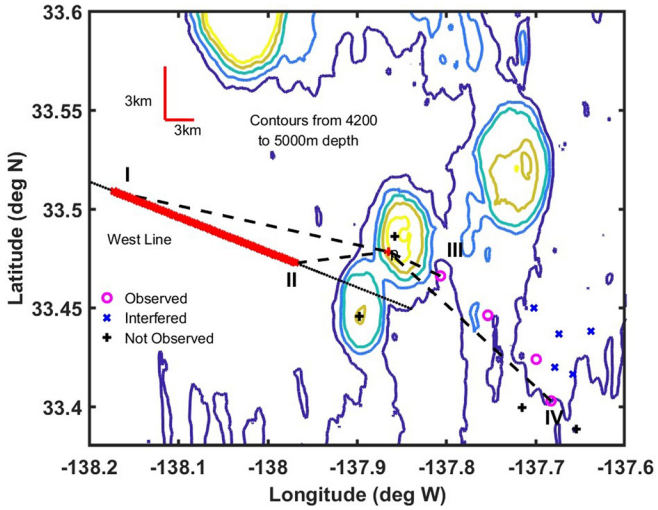

FIG. 6. (Color online) Incident and scattered azimuths and ranges for BDSRs from diffractor "p" at 77.5 Hz. BDSR-p was ensonified in an 11° swath of azimuths and energy was diffracted into a 12° swath of azimuths. See Table III for ranges and azimuths of paths I, II, III, and IV.

At 77.5 Hz, scattered energy from diffractor "p" is observed distinctly at receivers SP3, SP4, SP5, and SP6 (Fig. 6). For these four OBSs it was observed equally well on the hydrophone and vertical channels (including the hydrophone modules on SP3 and SP4). It was also observed on both horizontal channels on SP5 and SP6 but not on the horizontal channels on SP4. Only one horizontal channel on SP3 observed the diffraction. The BDSR is not observed at receivers SP7, SP8, LPC, and LPB. It interferes with the first water multiple (BRSR) for the other receivers including all elements of the DVLA. The scattered energy is observed at scattered ranges from 5.6 to 18.8 km from the diffractor to the receivers.

On OBS SP4 (Fig. 7), the BDSR-p arrival interferes with, and is indistinguishable from, the first water multiple (BRSR) around observed range 25 km, or incident range about 9.7 km from the diffractor. At ranges shorter than this the predicted BDSR arrival times are significantly different from the water multiple (BRSR) arrival time, but no BDSRs are observed. At very short observed ranges (less than 15 km) from the receiver the BDSR paths would correspond to backscatter from the diffractor.

V. BDSR ON NPAL04 AND OBSANP

One issue that arose during our analysis is whether or not the diffractor observed on the side of Seamount B on OBSANP (diffractor "p" in Figs. 3, 4, and 6) is the same as the diffractor observed at approximately the same location

TABLE III. Incident and difffracted azimuths and ranges for BDSRs from diffractor "p."

Identifier (Fig. 6)	Description	Range (km)	Azimuth (°)
I	Longest incident path	28.7	97
II	Shortest incident path	9.7	86
III	Shortest diffracted path	5.6	104
IV	Longest diffracted path	18.8	116

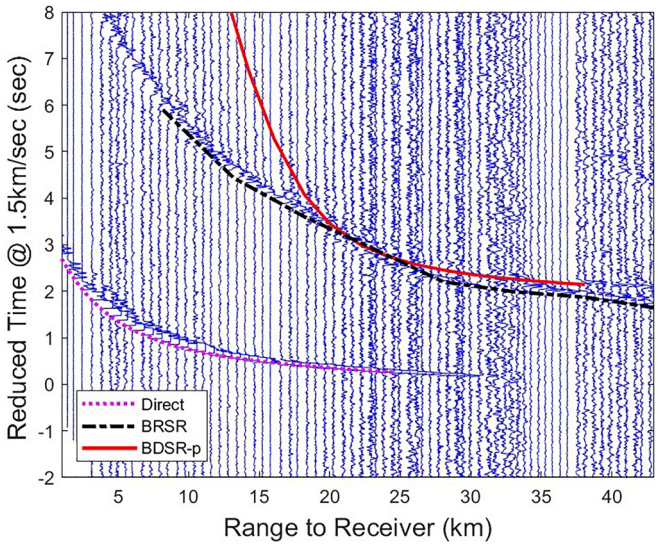

FIG. 7. (Color online) Received traces for 77.5 Hz transmissions from the west line to the hydrophone channel on SP4 at 77.5 Hz. Predicted arrival times for the direct, first multiple (BRSR) and BDSR-p arrivals are overlain on the traces. Clear BDSR-p arrivals appear after the first water multiple (BRSR) beyond 37 km range.

on NPAL04 (Fig. 8). This is a resolution issue which depends on the accuracy of locating diffractors on the NPAL04 and OBSANP experiments. (See Sec. VII A for a detailed discussion of the relevant resolutions.)

The NPAL04 location was based on 68.2 Hz transmissions from a single range (500 km) and the "error surfaces"

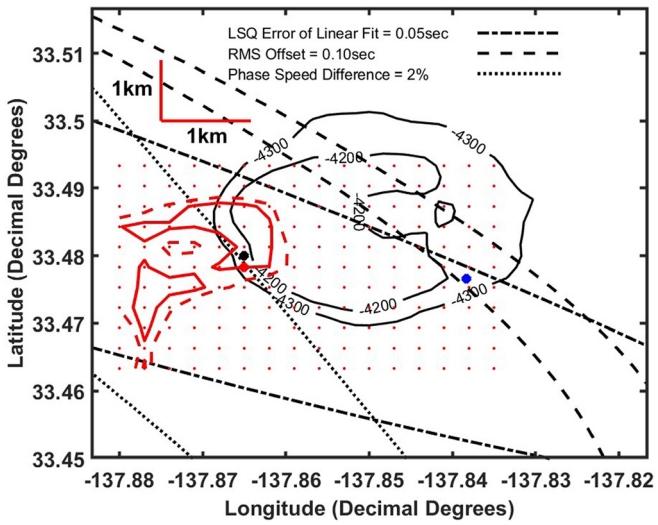

FIG. 8. (Color online) This figure compares the diffractor location analysis from NPAL04 (bold lines and large dots) and from the OBSANP experiment (thin lines and small dots). See Stephen *et al.* (2013) for a discussion of the three NPAL04 error surfaces and the depth constraint (4200–4300 m). No single point satisfies all four criteria. Points "1" (the southernmost large dot on the west side of the seamount) and "2" (the large dot on the east side of the seamount) were discussed as possible locations for the NPAL04 diffractor. Test points for the OBSANP BDSR location (small dots, separated by 0.003 deg which is about 330 m in latitude and somewhat less in longitude) are overlain on the summary of the NPAL04 error surfaces. For each test point the RMS error between the predicted and observed BDSR arrival times was computed. Solid and dashed thin contours indicate RMS errors of 0.04 and 0.06 s, respectively. The northernmost large dot on the west side of the seamount is the location of diffractor "p" for Figs. 3, 4, 6, 7, and 9.

were three measures of the travel time versus range curves for arrivals from the diffractor point on Seamount B to three OBSs and the DVLA (Stephen *et al.*, 2013). The three measures were: (i) the least square error of the linear regression of the observed arrival times, (ii) the RMS offset of the observed arrival times from the ray-predicted arrival times, and (iii) the difference in horizontal phase speed between the observed and ray-predicted arrival times. Given the similarity in relative BDSR arrival times for all ranges from 500 to 2400 km to the relative PE predicted arrival times at the DVLA hydrophone at 4250 m depth, we assumed that the diffractor point should be between 4200 and 4300 m depth. These four measures are summarized in Fig. 8 (based on Fig. 10 from Stephen *et al.*, 2013). No diffractor point meets all four criteria. In Stephen *et al.*, 2013 we chose two points on the side of Seamount B as possible locations. Point 1, to the west, meets all criteria except the RMS offset. Point 2, to the east, meets all criteria except the phase speed difference.

The OBSANP location was based on 77.5 Hz transmissions from 15 to 27 km on the west line to SP6, (Fig. 3) and the "error surface" was the RMS offset between the observed and ray-predicted arrival time (Fig. 8). The least error region (less than 0.04 s) has a radius of about 1 km and overlaps the location of Point 1 from the NPAL04 experiment. The analysis in Stephen *et al.* (2013) could not distinguish between Point 1 and Point 2, but Point 2 clearly does not explain the OBSANP arrival.

Elsewhere in the 2013 survey pairs of BDSRs were observed within a kilometer of each other (Fig. 4), so it is possible that the NPAL04 (Point 1) and OBSANP BDSR "p" arrivals arise from two distinct and unresolvable diffractors. It is quite likely however that the two diffractor points are the same. The location of the 2004 diffractor (Point 1) is sufficient to explain the arrival times of the BDSR from the 2013 diffractor within the resolution of the data.

VI. FREQUENCY DEPENDENCE OF BDSRS

BDSRs from diffractor "p" were also observed at 155 and 310 Hz. With the exception of one horizontal channel (GH1) on SP4 and SP5, 155 Hz diffractions were observed on all channels of SP3, SP4, SP5, and SP6. Interestingly 155 Hz diffractions were also observed on the long period OBSs LPB (SAIC hydrophone) and LPC (all channels) even though these broadband seismometers were not designed for such high frequencies. Weak 310 Hz diffractions were observed on the hydrophones on SP3, SP4, SP5, and SP6, but not on the inertial sensors. It is remarkable that these sensors observe any arrivals since they were acquired at 1000 sps, well below the sampling frequency for 310 Hz transmissions of 1240 sps (Table II). The hydrophone modules which did sample fast enough (1953.125 sps) had insufficient signal-to-noise ratios to observe BDSR-p. As examples of the frequency dependence, arrival time plots to the hydrophone channel on SP4 are shown in Fig. 7 for 77.5 Hz and in Fig. 9 for 155 and 310 Hz. More examples of the arrival time plots that show these features are given in the supplemental material.[1]

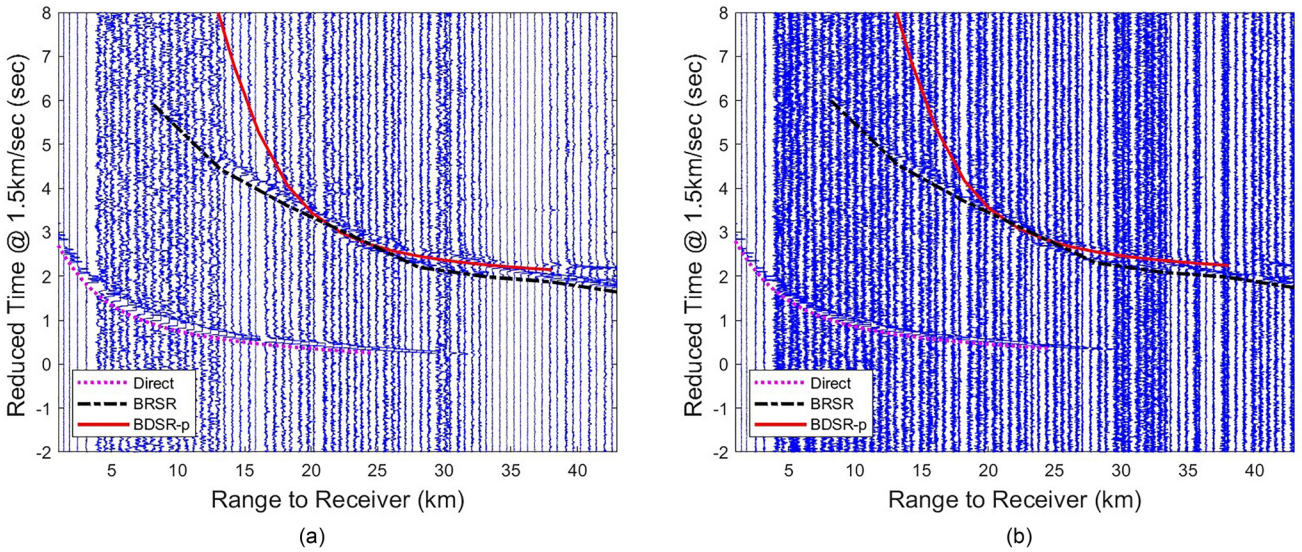

FIG. 9. (Color online) Received traces for (a) 155 Hz and (b) 310 Hz transmissions from the west line to the hydrophone channel on SP4. Predicted arrival times for the direct, first multiple (BRSR) and BDSR-p arrivals are overlain on the traces. Clear BDSR-p arrivals appear after the first water multiple (BRSR) beyond 37 km range.

VII. DISCUSSION

A. Resolutions

Five resolutions are considered in the paper: (i) the resolution of the time compressed signals (in time and range), (ii) the resolution of the NPAL04 and OBSANP experiments to locate diffractors (usually diffractor "p," but also the separation between two BDSRs seen on the same arrival time plot), (iii) the resolution of the navigation (How well are the sources, at a given time, and receivers located?), (iv) the resolution of the moving source during a transmission, and (v) the resolution of the bathymetry. In addition the length scale of diffraction and scattering processes is on the order of a wavelength (about 20, 10, and 5 m for the 77.5, 155, and 310 Hz transmissions, respectively).

The theoretical resolutions in range of the time compressed signals on OBSANP are about 40, 40, and 20 m, respectively, for the 77.5, 155, and 310 Hz transmissions (Table II). All of the BDSR locations discussed in this paper were made using the 77.5 Hz data. The theoretical resolution of the NPAL04 transmissions used in the BDSR triangulation is also about 40 m (Stephen *et al.*, 2013).

The analysis of the NPAL04 data did not distinguish between two, equally probable, diffractor locations (Fig. 8) separated by 2.5 km. The location error for diffractor "p" on OBSANP is given by the size of the error surface at 0.040 s (a little larger than the theoretical resolution of the 77.5 Hz time compressed signals, to allow for errors in picking BDSR arrival times). This is about 1.5 km east–west and 2 km north–south (Fig. 8). It is reasonable to assume that all of the additional 44 diffractor points in Fig. 4 would have similar resolutions. Occasionally two closely spaced diffractors can be identified on the same arrival time plot. Using the relative arrival time separation two distinct diffractors as close as 700 m can be resolved (Stephen *et al.*, 2017). A single diffractor point is consistent within the resolution of the NPAL04 and OBSANP experiments.

The ship was navigated with a global positioning system (GPS) and the location of the GPS antenna was monitored throughout the experiment to less than 4 m. Allowing for motion of the ship due to wind, waves, and swell, the offset of the source with respect to the antenna, etc. and doing some smoothing over time we estimate that at a given time the source location is known within 10 m.

The seafloor instruments were located by acoustic triangulation from the ship. Since the instruments are stationary we can use long time durations and many fixes to determine the location. We estimate that the receiver locations are also within 10 m (Table I). (The location of the vertical array as it moved with the currents was monitored during the experiment but we did not correct for this motion in our analysis.)

On NPAL04, the BDSRs were identified using point stationary sources. On OBSANP the source was towed at two knots and travelled 0.3 km between the start of each duty cycle. During the 77.5, 155, and 310 Hz transmissions the source travelled 109, 109, and 54 m, respectively. Four M-sequences were transmitted for each frequency at each source point and the received sequences were stacked to produce the traces displayed in the arrival time plots (for example, Fig. 3). So the point source, which is assumed fixed in the arrival time analysis, moved about 109 m during the displayed receptions.

The processing of the multibeam bathymetric data is discussed in detail in the cruise report (Stephen *et al.*, 2014). The shipboard multibeam system provides an image of the seafloor relief to about 10 km either side of the ship. This raw, unmerged data, acquired at a frequency of 12 kHz, has an approximate resolution of 50 m along- and across-track. Of course, the ship transitted over a given area many times during the experiment at different speeds and azimuths. In addition multi-beam data is available from previous expeditions to the site. So a bathymetric map like Fig. 4 is a composite product obtained by "merging" many transects and surveys from a number of cruises and ships. Poor data

must be edited out and the remaining data, containing many images of the same area of seafloor must be averaged and smoothed. All of the maps in this paper (except Fig. 8) display contours from the same composite, merged data set with a grid interval of 200 m. So what is the smallest feature that can be resolved with data on a 200 m grid? You might see the inflection of a contour based on two points (400 m) but you would need about ten points to outline a small seamount (2 km). These maps are good for identifying small seamounts, relatively featureless seafloor and bathymetric lineations. They are not adequate for imaging the wavelength scale structures (20 m or less) that are most likely responsible for the diffractions or scattering of BDSRs.

The receiver depths in Table I were determined by interpolating the multibeam bathymetry for the given receiver location. We estimate that the error bars on these depths are +/−5 m.

Stephen *et al.* (2017) show an example of raw, single swath, unmerged multibeam data with an improved approximate resolution of 60 m × 50 m. The map clearly shows the approximately north–south lineations in the "featureless seafloor" to the south–east of the receivers, but there is still no correlation of BDSR diffractor locations with seafloor structure.

The "point" diffractor, or scattering, region could be as small as 200 m but we are only able to locate it with an error of +/−1 km (Fig. 8) and we would be unlikely to resolve it with available bathymetric data (either merged, for example Fig. 4, or unmerged). Given the acoustic wavelengths there could be, and very likely are, many scatterers or diffractors within the diffracting region.

It is unlikely that the BDSRs are excited by specular reflection from facets. For specular reflection from a facet to be distinguished from a diffraction requires that the facet be many wavelengths on a side (Stephen and Swift, 1994). At 77.5 Hz, even five wavelengths would be 100 m and a facet this size or bigger should be resolvable with available bathymetry.

B. Diffraction mechanism

The mechanism within the 200 m-scale scattering region which focuses energy away from Snell's law angles is unknown but it could be (i) scattering from a random distribution of roughness elements or volume heterogeneities, (ii) scattering from a regular distribution of roughness elements or volume heterogeneities (analogous to Bragg diffraction), or (iii) simple diffraction from a single roughness element or volume heterogeneity.

It is not possible to predict the existence of BDSRs from the available bathymetry. At some point high-resolution bathymetric and bottom profiling surveys should be carried out around selected diffractor sites to determine the geologic structures responsible for the observed BDSRs.

C. Long- and short-range BDSRs

For long-range propagation (for example, greater than 500 km as on NPAL04) where the energy is focused in the sound channel (above the conjugate depth), the diffractor sites on the sides of small seamounts which protrude to the conjugate depth are most relevant. Whether the diffractor sites on small seamounts are excited or not will depend on the characteristics of the long range propagation, subject to the vagaries of oceanic processes and sound speed. For short range propagation (less than 50 km), since the whole seafloor is excited by direct wave energy (for example at ranges less than 17 km) even diffractors on the featureless deep seafloor are relevant. The BDSR mechanism provides coherent energy in addition to BRSR for ranges beyond lift-off of the direct wave.

D. Future work

We hope this study will prompt further modeling work to place bounds on the sorts of seafloor structures that could excite BDSRs. Since BDSRs do not satisfy Snell's law, given the available resolution of the bathymetry, they cannot be modelled using traditional three-dimensional long-range propagation codes such as parabolic equation methods, wavenumber integral methods or ray methods. Codes based on finite-element or finite-differences that handle scattering and diffraction from wavelength size heterogeneities, ideally in three-dimensions, are necessary (for example, Isakson and Chotiros, 2011; Stephen and Swift, 1994). Since these codes are computationally intensive a hybrid code, for example using ray methods down to and back from the diffracting region would be a reasonable approach. In this paper we have quantified the geometry (ranges, angles, and frequencies) for one BDSR to constrain the modeling work.

Analysis similar to Sec. IV, determining the three-dimensional geometry, including quantifying the BDSR amplitude and coherence should be done for the remaining 44 BDSR locations.

The two remaining phases of the OBSANP experiment, (i) an array of station stops within 50 km of the receivers, and (ii) a long line of station stops and underway transmissions to 250 km, should still be analyzed. The available DVLA data should be analyzed to provide vertical information on the role of BDSRs in signal receptions and ambient noise between the conjugate depth and the seafloor (for example, Farrokhrooz *et al.*, 2017).

E. T-phases

The BDSR mechanism is a controlled source reciprocal of the T-phase problem in marine seismology (Williams *et al.*, 2006). The T-phase (or T-wave or tertiary wave) from an earthquake in the oceanic crust and upper mantle is a hydroacoustic wave (∼10–100 Hz) that travels at the sound speed in water (∼1.5 km/s). It arrives at an oceanic or coastal sensor after the P- (primary) and S- (secondary) body waves which propagate through the Earth at higher speeds (typically 4.0–8.0 km/s for P-waves and 2.3–4.6 km/s for S-waves). Ray tracing from an earthquake epicenter at 4.0 km depth where the P and S speeds are quite large shows that, even for horizontal rays at the source, rays at the seafloor and in the ocean are near vertical. Yet to couple energy into the sound channel low grazing rays are required. Seafloor scattering has been invoked to explain the coupling when the seafloor is above

the conjugate depth. But many T-phases are observed when the surrounding seafloor is below the conjugate depth (see Fig. 3 of Williams *et al.*, 2006). So when the T-phase is excited in water deeper than the conjugate depth vertically propagating energy near the source couples into low grazing angle, long range propagation in the sound channel. For the BDSR mechanism in water deeper than the conjugate depth, long range propagation in the sound channel couples into near vertical propagation at the receiver.

VIII. CONCLUSIONS

Although they are present throughout the water column, BDSRs in general are most significant for receivers below the conjugate depth where acoustic energy from distant sources of signals and noise decreases. When observed at ranges less than 50 km their amplitude can be of the same order as the amplitude of BRSR (the first water multiple) arrivals.

We have presented a map (Fig. 4) of the OBSANP diffractor locations for the BDSRs observed on eight radial lines out to ranges of 50 km. Based on the NPAL04 experience we expected to observe only two or three diffractors and we expected all of them to be on the sides of seamounts with significant relief (hundreds of meters). It is surprising to us to observe so many diffractors (45 within a 25 km radius region or roughly one in every 40 km^2) and to observe that many of them are situated on relatively featureless seafloor. Most of the observed BDSRs are located out of the source–receiver sagittal plane and are true three-dimensional bottom diffraction phenomena.

The location of one of the two estimated 2004 NPAL04 diffraction points (BDRS observed from 500 to 3200 km range) can explain OBSANP BDSR "p" (observed at source–receiver ranges from 15 to 35 km) within the resolution of the data. It is quite likely that the same geological feature diffracted the energy in the two experiments. BDSRs are repeatable, discrete, and deterministic features for deep water propagation from 15 to 3200 km range.

BDSR "p" was excited at incident ranges from 9.7 to 28.7 km, corresponding to low grazing angles and even angles beyond lift-off (evanescent excitation). It was excited over a swath of 11° azimuth. Scattered energy from diffractor "p" was observed at relatively short ranges from 5.6 to 18.8 km, corresponding to large to small, but finite, grazing angles. Energy from diffractor "p" was scattered into a 12° swath of azimuths.

BDSR "p" is observed at transmissions of 77.5, 155, and 310 Hz. BDSRs can be robust features over two octaves. They are not ephemeral, random scattering.

ACKNOWLEDGMENTS

We greatly appreciate the support from Captain Curl, the officers, and crew of the R/V Melville (MV1308). The OBS data used in this research was acquired on instruments from the ocean bottom seismograph instrument pool (OBSIP) at Scripps Institution of Oceanography. Ernie Aaron (SIO) was responsible for shipboard OBS operations. The multi-beam data was processed using the MB-System (Caress and Chayes, 1996). Figure 1 was prepared using the generic mapping tool (Wessel and Smith, 1998). Feedback and reviews from an anonymous reviewer and the editorial staff of JASA are also greatly appreciated. The OBSANP experiment was funded by the ONR Ocean Acoustics Program (Code 322 OA) under Grant Nos. N00014-10-1-0987 and N00014-10-1-0510. Analysis was carried out under ONR Grant Nos. N00014-14-1-0324, N00014-16-1-2337, and N00014-17-C-7043.

APPENDIX: SEMANTICS OF DIFFRACTION AND SCATTERING

There can be some confusion between the terms "scattering" and "diffraction" as used in the ocean acoustics community. The Oxford English Dictionary (2018a) defines "diffraction" in optics as "The process by which a beam of light is spread out or bent after passing through a slit or across the edge of an opaque body, typically accompanied by interference of the waveforms that result." And in physics as "An analogous phenomenon occurring when waves of any kind…are spread out as a result of passing through a slit or across the edge of an obstacle." These definitions describe "bending diffraction."

But there is also "scattering diffraction" as included in the more general definitions of the following:

(i) Keller (1962)—"These [diffracted] rays are produced by incident rays which hit edges, corners, or vertices of boundary surfaces, or which graze such surfaces."
(ii) Pierce (1989) on page 424—"The term [diffraction phenomena] as used here applies to contexts where major features of the propagation and of the overall acoustic field are well described by ray-acoustic concepts. Diffraction is then the label assigned to those features of the field which the ray model fails to explain."
(iii) Pierce (1989) on page 378—"A diffracted ray is a ray which originates at an interface, a surface, or an edge and which propagates with all of the attributes of a ray generated by a real source but which is created by a process inexplicable (and therefore labeled as diffraction) within the confines of the ordinary geometrical acoustics theory."

The discipline of multichannel seismology uses the concept of "scattering diffraction" almost exclusively:

(i) Ikelle and Amundsen (2005)—"The subsurface is composed of more than reflections: it also includes faults, simple and complex folds, pinchouts, unconformities, and so on. In many instances, the laws of reflection and refraction are inadequate, because the energy is diffracted, rather than reflected or refracted."
(ii) Evans (1997)—"Diffractions occur at sharp discontinuities, such as at the edge of a bed, fault, or geologic pillow."

In contrast simple "scattering" in physics is defined by the Oxford English Dictionary (2018b) as "Of a surface, semi-opaque substance: To throw back (light) brokenly in all directions. More widely, to deflect, diffuse, or reflect (radiation, particles, or the like) in a more or less random fashion."

In this paper, we are not considering "bending diffraction" at all. We use the terms "scattering" and "diffraction" more or less interchangeably and are quite comfortable with the notion of "scattering diffraction" to distinguish it from "bending diffraction." The use of these terms is consistent with the definitions given above.

"Diffraction" is used in the context of a deterministic process from a "discrete" point location. For example a point heterogeneity in a homogeneous medium diffracts energy. "Scattering" implies a random acoustic field and/or random heterogeneities or roughness. For example at frequencies around 12 kHz there is monostatic backscatter from most of the seafloor, as exploited by multibeam bathymetry. Given the resolution of the OBSANP bathymetry (∼200 m) a "point" can be a number of wavelengths (about 20 m at 77.5 Hz) in size.

[1]See supplementary material at https://doi.org/10.1121/1.5125427 for more examples of arrival time plots like Figs. 3, 7, and 9.

Baggeroer, A. B., and Kuperman, W. A. (**1983**). "Matched field processing in ocean acoustics," in *Acoustic signal processing for ocean exploration*, edited by J. M. F. Moura and I. M. G. Lourtie (Kluwer, Dordrecht), pp. 79–114.

Berger, J., Bidlot, J.-R., Dzieciuch, M. A., Farrell, W. E., Worcester, P. F., and Stephen, R. A. (**2018**). "A deep ocean acoustic noise floor, 1–800 Hz," J. Acoust. Soc. Am. **143**, 1223–1233.

Birdsall, T. G. (**1976**). "On understanding the matched filter in the frequency domain," IEEE Trans. Educ. **19**, 168–169.

Birdsall, T. G., and Metzger, K. (**1986**). "Factor inverse matched filtering," J. Acoust. Soc. Am. **79**, 91–99.

Birdsall, T. G., Metzger, K., and Dzieciuch, M. A. (**1994**). "Signals, signal processing, and general results," J. Acoust. Soc. Am. **96**, 2343–2352.

Butler, R., and Lomnitz, C. (**2002**). "Coupled seismoacoustic modes on the seafloor," Geophys. Res. Lett. **29**, 57-1–57-4, https://doi.org/10.1029/2002GL014722.

Caress, D. W., and Chayes, D. N. (**1996**). "Improved processing of hydrosweep DS multibeam data on the R/V Maurice Ewing," Mar. Geophys. Res. **18**, 631–650, https://doi.org/10.1007/BF00313878.

Chapman, N. R., and Marrett, R. (**2006**). "The directionality of acoustic T-phase signals from small magnitude submarine earthquakes," J. Acoust. Soc. Am. **119**, 3669–3675.

de Groot-Hedlin, C. D., and Orcutt, J. A. (**1999**). "Synthesis of earthquake-generated T-waves," Geophys. Res. Lett. **26**, 1227–1230, https://doi.org/10.1029/1999GL900205.

Evans, B. J. (**1997**). "A handbook for seismic data acquisition in exploration," in *Geophysical Monograph Series, 7*, edited by D. V. Fitterman (Society of Exploration Geophysics, Tulsa, OK), 305 pp.

Farrell, W. E., Berger, J., Bidlot, J.-R., Dzieciuch, M., Munk, W., Stephen, R. A., and Worcester, P. F. (**2016**). "Windsea behind a cold front and deep ocean acoustics," J. Phys. Oceanogr. **46**, 1705–1716.

Farrokhrooz, M., Wage, K. E., Dzieciuch, M. A., and Worcester, P. F. (**2017**). "Vertical line array measurements of ambient noise in the North Pacific," J. Acoust. Soc. Am. **141**, 1571–1581.

Golomb, S. W. (**1982**). *Shift Register Sequences* (Aegean Park Press, Laguna Hills, CA), 247 pp.

Ikelle, L. T., and Amundsen, L. (**2005**). "Introduction to petroleum seismology," in *Investigations in Geophysics*, edited by M. R. Cooper and A. F. Gangi (Society of Exploration Geophysics, Tulsa, OK),Vol. 12, p. 679.

Isakson, M. J., and Chotiros, N. P. (**2011**). "Finite element modeling of reverberation and transmission loss in shallow water waveguides with rough boundaries," J. Acoust. Soc. Am. **129**, 1273–1279.

Keller, J. B. (**1962**). "A geometrical theory of diffraction," J. Opt. Soc. Am. **52**, 116–130.

McPeak, S. P., D'Spain, G. L., Stephen, R. A., von der Heydt, K., and Worcester, P. F. (**2013**). "OBSANP data acquisition system: Operator's manual and system overview," *WHOI-2013-06* (Woods Hole Oceanographic Institution, Woods Hole, MA), 54 pp.

Mercer, J. A., Colosi, J. A., Howe, B. M., Dzieciuch, M. A., Stephen, R., and Worcester, P. F. (**2009**). "LOAPEX: The long-range ocean acoustic propagation experiment," IEEE J. Ocean. Eng. **34**, 1–11.

Metzger, K. M., Jr. (**1983**). "Signal processing equipment and technique for use in measuring ocean acoustic multipath structures," Ph.D. thesis, University of Michigan, Ann Arbor, MI, 338 pp.

Munk, W., Worcester, P., and Wunsch, C. (**1995**). *Ocean Acoustic Tomography* (Cambridge University Press, Cambridge, UK), 456 pp.

Okal, E. (**2008**). "The generation of T waves by earthquakes," Adv. Geophy. **49**, 2–65.

Oxford English Dictionary. (**2018a**). Oxford University Press, http://www.oed.com/view/Entry/52519?redirectedFrom=diffraction (Last viewed 16 October 2018).

Oxford English Dictionary (**2018b**). Oxford University Press, http://www.oed.com/view/Entry/172162?rskey=4FhP0A&result=2 (Last viewed 16 October 2018).

Pierce, A. D. (**1989**). *Acoustics: An Introduction to Its Physical Principles and Applications* (Acoustical Society of America, Woodbury, NY), 678 pp.

Stephen, R., Worcester, P., Bolmer, S., Swift, S., Udovydchenkov, I., and Dzieciuch, M. (**2017**). "Bottom-diffracted surface-reflected arrivals in the North Pacific," in *UACE2017 4th Underwater Acoustics Conference and Exhibition*, edited by J. S. Papadakis (Institute of Applied and Computational Mathematics, Foundation for Research and Technology–Hellas, Nikolaou Plastira 100, Vassilika Vouton, GR 700 13 Heraklion, Crete, Greece), pp. 587–594.

Stephen, R. A., Bolmer, S. T., Dzieciuch, M. A., Worcester, P. F., Andrew, R. K., Buck, L. J., Mercer, J. A., Colosi, J. A., and Howe, B. M. (**2009**). "Deep seafloor arrivals: An unexplained set of arrivals in long-range ocean acoustic propagation," J. Acoust. Soc. Am. **126**, 599–606.

Stephen, R. A., Bolmer, S. T., Udovydchenkov, I. A., Dzieciuch, M. A., Worcester, P. F., Andrew, R. K., Mercer, J. A., Colosi, J. A., and Howe, B. M. (**2013**). "Deep seafloor arrivals in long range ocean acoustic propagation," J. Acoust. Soc. Am. **134**, 3307–3317.

Stephen, R. A., and Swift, S. A. (**1994**). "Modeling seafloor geoacoustic interaction with a numerical scattering chamber," J. Acoust. Soc. Am. **96**, 973–990.

Stephen, R. A., Worcester, P. F., Udovydchenkov, I. A., Aaron, E., Bolmer, S. T., Carey, S., McPeak, S. P., Swift, S. A., and Dzieciuch, M. A. (**2014**). "Ocean bottom seismometer augmentation in the North Pacific (OBSANP)—Cruise report," *WHOI-2014-3* (Woods Hole Oceanographic Institution, Woods Hole, MA), 246 pp.

Wessel, P., and Smith, W. H. F. (**1998**). "New, improved version of generic mapping tools released," EOS Trans. Am. Geophys. Union **79**, 579–579.

Williams, C. M., Stephen, R. A., and Smith, D. K. (**2006**). "Hydroacoustic events located at the intersection of the Atlantis and Kane Transform Faults with the Mid-Atlantic Ridge," Geochem. Geophys. Geosys. **7**, 1–28.

Yang, Y., and Forsyth, D. W. (**2003**). "Improving epicentral and magnitude estimation of earthquakes from T Phases by considering the excitation function," Bull. Seismol. Soc. Am. **93**, 2106–2122.